General Relativity and Gravitation (2023) 55:115
https://doi.org/10.1007/s10714-023-03160-1

RESEARCH

Exploring the possibility of interacting quintessence model as an alternative to the ΛCDM model

Nandan Roy[1]

Received: 22 July 2023 / Accepted: 26 September 2023

Abstract

This study examines interacting quintessence dark energy models and their observational constraints for a general parameterization of the quintessence potential, which encompasses a broad range of popular potentials. Four different forms of interactions are considered. The analysis is done by expressing the system as a set of autonomous equations for each interaction. The Bayesian Model Comparison has been used to compare these models with the standard Lambda Cold Dark Matter (ΛCDM) model. Our analysis shows positive and moderate evidence for the interacting models over the ΛCDM model. We also report the status of the Hubble tension for these models, even though there is an increment in the best-fit value of the Hubble parameters, these models can not resolve the Hubble tension.

Keywords Dark energy · Dark matter · Quintessence · Hubble tension

Contents

1 Introduction
2 Mathematical background
3 The interaction
3.1 Interaction I ($Q = \beta\rho_m\dot{\phi}$)
3.2 Interaction II ($Q = \beta\rho_\phi\dot{\phi}$)
3.3 Interaction III ($Q = \beta\rho_m\sqrt{\rho_\phi}\dot{\phi}/H$)
3.4 Interaction IV ($Q = \beta\dot{\phi}H^2 w_\phi$)
4 Numerical simulations
4.1 Initial condition
4.2 Observational data
4.2.1 SN-Ia data
4.2.2 Baryon acoustic oscillation
4.2.3 Compressed planck likelihood

✉ Nandan Roy
nandan.roy@mahidol.ac.th

[1] Centre for Theoretical Physics and Natural Philosophy, Mahidol University, Nakhonsawan Campus, Phayuha Khiri, Nakhonsawan 60130, Thailand

Published online: 15 October 2023

4.3 Observational constraints . . . . . .
4.4 Comparison with ΛCDM . . . . . .
5 Conclusions . . . . . .
References . . . . . .

1 Introduction

The accelerated expansion of the universe has been confirmed by various cosmological observations [1–5] but the reason behind it remains a mystery. Cosmological constant [6] is considered as the simplest and most successful candidate for dark energy, but it still faces major theoretical challenges like the cosmological constant problem and the coincidence problem.

Recent high-precision cosmological data has shown a statistically significant discrepancy in the estimation of the current value of the Hubble parameter (H_0) between early-time and late-time observations, which poses another challenge to the cosmological constant. Early universe measurements like CMB Planck collaboration [7] (including BAO [8, 9], BBN [10]) and DES [11–13] collaboration estimate $H_0 \sim (67.0 - 68.5)$ km/s/Mpc, while late-time distance ladder measurements like SH0ES [14] and H0LiCOW [15] collaborations using time-delay cosmography method report $H_0 = (74.03 \pm 1.42)$ km/s/Mpc. Over the years this discrepancy has increased of the order of $\simeq 5.3\sigma$ [16], indicating the possibility of new physics beyond ΛCDM in the dark energy sector.

Dynamical dark energy models, such as quintessence, k-essence, phantom dark energy, etc., have been proposed as alternatives to the cosmological constant [17, 18]. These models involve a scalar field with a potential energy that drives the accelerated expansion of the universe, and the equation of state of the dark energy evolves with time [19–28]. **Apart from these scalar field models a wide variety of other models has been introduced which can reduce or alleviate Hubble tension like early dark energy model** [29], **running vacuum model** [30–33], **phantom crossing models** [22, 34]**, etc.** The possibility of interactions between dark matter and dark energy in dynamical dark energy models is not ruled out from both theoretical and observational perspectives. Interactions between the dark sectors have been shown to alleviate the cosmic coincidence problem [35–39], and in recent years, interacting models have gained attention for their potential to resolve the H_0 and σ_8 tensions [40–47].

In cosmology, the interaction between dark matter and dark energy is considered by introducing some unknown interaction terms into the continuity equation. It has been proposed that the dark matter and dark energy components are not conserved separately but instead conserved jointly. The form of the interaction is arbitrary and is generally chosen based on its phenomenological performance. The consideration of the interaction between the dark sectors should affect the expansion history and overall evolution of the universe [38]. Numerous studies have extensively explored the cosmological ramifications arising from the interactions between dark matter and dark energy [36, 48–54]. These investigations encompass a broad range of perspectives, including both theoretical considerations and observational analyses.

Dynamical systems analysis has been extensively used to examine the qualitative behavior of various cosmological models, including interacting dark energy models. Generally, one can convert the Einstein field equations, along with the interaction term, into a set of autonomous equations and employ dynamical systems analysis techniques to investigate the stability of these models. Previous studies have already explored models with different types of interactions, encompassing both general relativity and modified gravity models [55–60]. For a comprehensive understanding of the dynamical systems analysis of interacting dark energy models, we recommend referring to the following review: [61].

In this study, we analyzed the performance of interacting quintessence dark energy models using state-of-the-art cosmological data at the background level. We considered a very general setup of the quintessence potential by using the parametrization of the potential from [62], which includes a large class of potentials. Four distinct interaction terms were considered, and the Einstein field equations for the interacting quintessence field were reformulated into a set of autonomous equations through appropriate variable transformations. The models were then implemented in the Boltzmann code CLASS and evaluated against recent cosmological observations using the MCMC code Montepython. We employed the concept of Bayes factor and Jeffreys scale to compare these interacting models with each other and also with the ΛCDM model.

The structure of the present study is outlined as follows: In Sect. 2, we provide an overview of the mathematical formulation and the dynamics of the scalar field. Section 3 focuses on the mathematical setup for each type of interaction term considered. The initial conditions and the implementation of the model in the CLASS code, as well as the constraints obtained from recent cosmological observations, are described in Sect. 4. Finally, our results and findings are summarized in Sect. 5.

2 Mathematical background

Let us consider a spatially flat Friedmann-Robertson-Walker (FRW) universe that is composed of radiation, dark matter, and dark energy, with the latter two components interacting with each other. We consider quintessence scalar field as our chosen dark energy component and we further assume that the components of the universe are barotropic in nature and obey the relation $p_j = w_j \rho_j$, where $w_r = 1/3$ for radiation and $w_m = 0$ for dark matter. For the above-mentioned universe, the Einstein field equations are written as

$$H^2 = \frac{\kappa^2}{3}\left(\sum_j \rho_j + \rho_\phi\right), \tag{1a}$$

$$\dot{H} = -\frac{\kappa^2}{2}\left[\sum_j (\rho_j + p_j) + (\rho_\phi + p_\phi)\right], \tag{1b}$$

where, $\kappa^2 = 8\pi G$ and a is the scale factor of the Universe, while $H \equiv \dot{a}/a$ denotes the Hubble parameter, and the dot represents the derivative with respect to cosmic time. The continuity equations for each component, including radiation, matter, and the scalar field, can be expressed as follows:

$$\dot{\rho_r} + 3H\rho_r(1 + w_r) = 0, \tag{2a}$$
$$\dot{\rho_m} + 3H\rho_m(1 + w_m) = -Q, \tag{2b}$$
$$\dot{\rho_\phi} + 3H(\rho_\phi + p_\phi) = +Q. \tag{2c}$$

In this context, Q denotes the coupling between the quintessence field and the matter sector, and we have chosen a convention such that if Q is positive, the energy transfer occurs from dark matter to dark energy, whereas if Q is negative, the energy transfer occurs from dark energy to dark matter. The densities of radiation, matter, and the scalar field are represented by ρ_r, ρ_m, and ρ_ϕ, respectively, while their equation of state (EoS) is denoted as w_r, w_m, and w_ϕ. The wave equation for the scalar field can be expressed as follows:

$$\ddot{\phi} + 3H\dot{\phi} + \frac{dV(\phi)}{d\phi} = \frac{Q}{\dot{\phi}}, \tag{3}$$

where the potential of the scalar field is $V(\phi)$.

To write down the evolution equations of the quintessence field as an set of autonomous equation, we introduce the following set of dimensionless variables,

$$x \equiv \frac{\kappa\dot{\phi}}{\sqrt{6}H} = \Omega_\phi^{1/2}\sin(\theta/2), \tag{4a}$$
$$y \equiv \frac{\kappa V^{1/2}}{\sqrt{3}H} = \Omega_\phi^{1/2}\cos(\theta/2, \tag{4b}$$
$$y_1 \equiv -2\sqrt{2}\frac{\partial_\phi V^{1/2}}{H}, \tag{4c}$$
$$y_2 \equiv -4\sqrt{3}\frac{\partial_\phi^2 V^{1/2}}{\kappa H}. \tag{4d}$$

This particular transformation was first used in [63] and later it is used in [62]. Using these sets of new variables the system of equations that governs the dynamics of the scalar field reduces to the following set of autonomous equations,

$$\theta' = -3\sin\theta + y_1 + q\ \Omega_\phi^{1/2}\cos(\theta/2), \tag{5a}$$
$$y_1' = \frac{3}{2}(1 + w_{tot})\, y_1 + \Omega_\phi^{1/2}\sin(\theta/2)y_2, \tag{5b}$$
$$\Omega_\phi' = 3(w_{tot} - w_\phi)\Omega_\phi + q\ \Omega_\phi^{1/2}\sin(\theta/2), \tag{5c}$$

where $q = \frac{\kappa Q}{\sqrt{6}H^2\dot{\phi}}$ represents the interaction in the new system and a 'prime' is the differentiation with respect to the e-foldings $N = \ln(a)$. From now on we consider

the unit $\kappa^2 = 1$. The total EoS of the system is given as follows,

$$w_{tot} \equiv \frac{p_{tot}}{\rho_{tot}} = \sum_i w_i \Omega_i = \frac{1}{3}\Omega_r + \Omega_\phi w_\phi. \tag{6}$$

Here Ω_ϕ is the scalar field energy density parameter and the scalar field EoS is given by $w_\phi = -\cos\theta$. One can notice the system of equations in Eq.(5) is not closed until unless one consider a particular form of the y_2. In this work we will be considering the following form of the y_2;

$$y_2 = y\left(\alpha_0 + \alpha_1 y_1/y + \alpha_2 y_1^2/y^2\right). \tag{7}$$

This form of y_2 [62, 64] includes a large number of popular scalar field potentials and particularly important as one can study different classes of scalar field solutions without considering any particular form of the potential. The α parameters in the above expression of y_2 are called the active parameters which affect the dynamics of the scalar field.

3 The interaction

Although current observations allow for the possibility of an interaction between dark matter and dark energy, the precise form of this interaction remains unknown. In this study, we have explored the following four different forms of interactions (i) $Q = \beta\rho_m\dot{\phi}$, (ii) $Q = \beta\rho_\phi\dot{\phi}$, (iii) $Q = \beta\rho_m\sqrt{\rho_\phi}\dot{\phi}/H$, and (iv) $Q = \beta\dot{\phi}H^2 w_\phi$, here β is the coupling parameter. The choices of these specific forms of interaction are phenomenological and also intended to simplify the mathematics and facilitate the closure of the autonomous systems in Eq.(5).

3.1 Interaction I ($Q = \beta\rho_m\dot{\phi}$)

This interaction was first used in [65] and later in [48]. In this particular form of interaction the autonomous system of the scalar field dynamics will be reduced to the following;

$$\theta' = -3\sin\theta + y_1 + \sqrt{3/2}\beta\Omega_\phi^{1/2}(1-\Omega_\phi)\cos(\theta/2), \tag{8a}$$

$$y_1' = \frac{3}{2}(1+w_{tot})\,y_1 + \Omega_\phi^{1/2}\sin(\theta/2)y_2, \tag{8b}$$

$$\Omega_\phi' = 3(w_{tot} - w_\phi)\Omega_\phi + \sqrt{3/2}\beta\Omega_\phi^{1/2}(1-\Omega_\phi)\sin(\theta/2). \tag{8c}$$

The continuity equation of the matter sector in terms of the variables given in Eq.(4) can be written as

$$\dot{\rho_m} + 3H\rho_m = -\sqrt{6}\beta H \rho_m \sqrt{\Omega_\phi}\sin\theta/2 \tag{9}$$

3.2 Interaction II ($Q = \beta\rho_\phi\dot{\phi}$)

Though not exact a similar form has been considered in [66] (see the references there in also). For this particular choice of interaction the autonomous system reduces to the following;

$$\begin{aligned}
\theta' &= -3\sin\theta + y_1 \\
&\quad + \sqrt{3/2}\beta\Omega_\phi^{3/2}\cos(\theta/2), && \text{(10a)}\\
y_1' &= \frac{3}{2}(1 + w_{tot})\, y_1 + \Omega_\phi^{1/2}\sin(\theta/2) y_2, && \text{(10b)}\\
\Omega_\phi' &= 3(w_{tot} - w_\phi)\Omega_\phi \\
&\quad + \sqrt{3/2}\beta\Omega_\phi^{3/2}\sin(\theta/2). && \text{(10c)}
\end{aligned}$$

Similar to the previous case the continuity equation of the matter sector reduces to the following;

$$\dot{\rho_m} + 3H\rho_m = -3\sqrt{6}\beta H^3 \sin(\theta/2)\Omega_\phi^{3/2} \tag{11}$$

3.3 Interaction III ($Q = \beta\rho_m\sqrt{\rho_\phi}\dot{\phi}/H$)

The autonomous system reduces to the following for this particular choice of interaction;

$$\begin{aligned}
\theta' &= -3\sin\theta + y_1 \\
&\quad + \frac{3}{\sqrt{2}}\beta\Omega_\phi(1 - \Omega_\phi)\cos(\theta/2), && \text{(12a)}\\
y_1' &= \frac{3}{2}(1 + w_{tot})\, y_1 + \Omega_\phi^{1/2}\sin(\theta/2) y_2, && \text{(12b)}\\
\Omega_\phi' &= 3(w_{tot} - w_\phi)\Omega_\phi \\
&\quad + 3/\sqrt{2}\beta\Omega_\phi(1 - \Omega_\phi)\sin(\theta/2). && \text{(12c)}
\end{aligned}$$

The continuity equation for the matter sector can be written as

$$\dot{\rho_m} + 3H\rho_m = -3\sqrt{2}\beta H \rho_m \Omega_\phi \sin\theta/2. \tag{13}$$

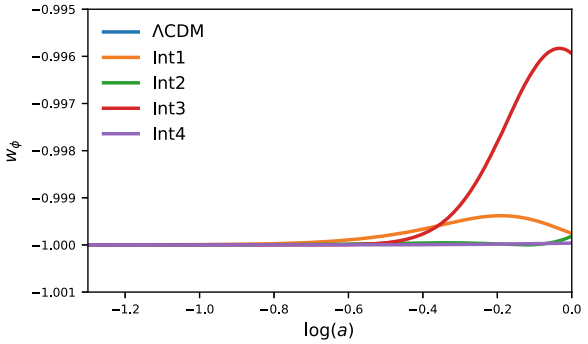

Fig. 1 Plot of the evolution of the scalar field EoS(w_ϕ) for different interaction forms with $\alpha_i = 0$ and other parameters set to their best fit value (see Table 1)

3.4 Interaction IV ($Q = \beta\dot{\phi}H^2 w_\phi$)

In this case, the autonomous system is reduced to the following;

$$\theta' = -3\sin\theta + y_1 - \frac{1}{\sqrt{6}}\beta\sqrt{\Omega_\phi}\cos(\theta)\cos(\theta/2), \tag{14a}$$

$$y_1' = \frac{3}{2}(1 + w_{tot})\, y_1 + \Omega_\phi^{1/2}\sin(\theta/2)y_2, \tag{14b}$$

$$\Omega_\phi' = 3(w_{tot} - w_\phi)\Omega_\phi - \frac{1}{\sqrt{6}}\beta\sqrt{\Omega_\phi}\cos(\theta)\sin(\theta/2). \tag{14c}$$

and the matter continuity equation takes the following form,

$$\dot{\rho_m} + 3H\rho_m = \sqrt{6}\beta H^3\sqrt{\Omega_\phi}\cos(\theta)\sin\theta/2. \tag{15}$$

In Fig. 1, we present the evolution of the equation of state (EOS) of the scalar field (w_ϕ) using the best-fit value of the β parameter obtained from the MCMC analysis (see Sect. 4.3) for each interacting model. We consider a general choice of $\alpha_0 = \alpha_1 = \alpha_1 = 0$. This particular choice of the α parameters corresponds to the potential taking the form $V(\phi) = (A + B\phi)^2$ (refer to Table II in [62]). However, it's important to note that different values of the α parameters can be selected, leading to distinct forms of the potential.

From the plots in Fig. 1, it can be observed that for all the interaction models, the evolution of the EOS is indistinguishable from that of a cosmological constant in the early times. However, at late times, the EOS deviates from the value $w_\phi = -1$.

In Fig. 2, we illustrate the evolution of the density parameters Ω_m and Ω_ϕ using the same choice of α parameters as in Fig. 1. It is noteworthy that, for all the interacting models, the evolution of Ω_m and Ω_ϕ cannot be distinguished from each other.

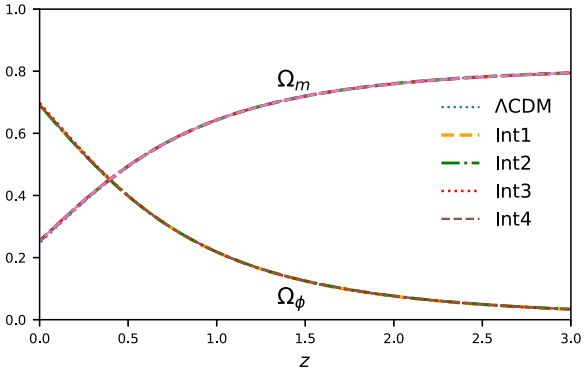

Fig. 2 Plot of the Ω_m and Ω_ϕ for the interacting models for $\alpha_i = 0$ and other parameters set to their best fit value (see Table 1)

4 Numerical simulations

4.1 Initial condition

To study the dynamics of the model numerically, we have implemented all the corresponding sets of autonomous equations for the four different interactions, along with the modified continuity equations, in the Boltzmann code CLASS [67–69]. To obtain reliable numerical solutions, it is important to provide a good guess for the initial conditions to the CLASS code. Following the prescription given in [70], we have estimated the initial conditions based on two different assumptions. The first assumption is that the dark energy equation of state is approximately $w_\phi \simeq -1$, leading to $\theta < 1$. The second assumption is that the contribution of the dark energy density during both matter and radiation domination is negligible, i.e., $\Omega_\phi \ll 1$. By considering approximate solutions during radiation and matter domination, and equating them at the radiation-matter equality epoch, we can obtain;

$$\theta_i \simeq \frac{9}{10} a_i^2 \frac{\Omega_{m0}^{1/2}}{\Omega_{r0}^{1/2}} \theta_0, \tag{16a}$$

$$\Omega_{\phi i} \simeq a_i^4 \frac{\Omega_{m0}}{\Omega_{r0}} \Omega_{\phi 0}, \tag{16b}$$

The initial value of the variable y_1 is related to the angular variable as $y_{1i} = 5\theta_i$. The initial condition for ρ_m is taken as $\rho_{mi} = \rho_{m0}(\frac{a_i}{a_0})^{-3}$. In the CLASS code, a_i is typically considered to be $\simeq 10^{-15}$.

4.2 Observational data

We utilized the MCMC parameter estimation code Montepython [71] to constrain the cosmological parameters. The data sets used for this purpose are the following;

4.2.1 SN-Ia data

The type Ia supernovae are commonly acknowledged as standard candles. Their relatively uniform absolute luminosity makes them extremely useful for measuring cosmological distances [1, 72]. Here we have used the Pantheon compilation sample of SN-Ia data, which was compiled in [73] and includes 1048 data points for SN-Ia. The complete numerical data for the Pantheon SN-Ia catalog is publicly accessible.[1] [2]

The redshift range for Pantheon samples is $0 < z < 2.3$. The distance modulus $\mu(z)$ of any type Ia Supernova located at a distance of redshift z is given as $\mu(z) = m - M$, where m represents its apparent magnitude and M is the absolute magnitude. Theoretically, the distance modulus can be written as

$$\mu_{th}(z) = 5\log_{10}\frac{d_L(z)}{(H_0/c)\,Mpc} + 25,$$

where H_0 is the current Hubble rate, c is the speed of light and $d_L(z)$ is the luminosity distance. The luminosity distance $d_L(z)$ in a spatially flat FRW universe is defined as

$$d_L(z) = (1+z)H_0\int_0^z \frac{dz'}{H(z')}.$$

The chi-square of the SN-Ia measurements,

$$\chi^2_{SN} = \Delta\mu^T \cdot \mathbf{C}^{-1}_{SN} \cdot \Delta\mu.$$

$\mathbf{C}_{SN}$ is a covariance matrix, and $\Delta\mu = \mu_{obs} - \mu_{th}$, μ_{obs} corresponds to the measured distance modulus of a particular SNIa. Now the distance modulus can be estimated from the observation of light curves using the empirical formula,

$$\mu_{obs} = m_B - M + \alpha X_1 - \beta C + \Delta_M + \Delta_B,$$

Here, m_B is the observed peak magnitude of the SNIa in the rest frame of the B band, and M is the absolute B-band magnitude of a fiducial SNIa. The parameters α and β are coefficients that relate the luminosity of the SNIa to its time stretching (X_1) and color (C), respectively. Additionally, Δ_M is a distance correction based on the host-galaxy mass of the SNIa, and Δ_B is a correction based on predicted biases from simulation.

Moreover, the total covariance matrix $\mathbf{C}_{SN}$ is defined as the sum of the statistical matrix D_{stat} and the systematic matrix C_{sys}, as shown by the equation

$$\mathbf{C}_{SN} = D_{\text{stat}} + C_{\text{sys}}$$

[1] http://dx.doi.org/10.17909/T95Q4X.

[2] https://archive.stsci.edu/prepds/ps1cosmo/index.html.

The statistical matrix D_{stat} is a diagonal matrix that contains the distance error of each supernova type Ia (SNIa) along its main diagonal. The distance error is composed of several sources of uncertainty, such as the photometric error, the mass step correction, the peculiar velocity and redshift measurement, the gravitational lensing, the intrinsic scatter, and the distance bias correction. These sources of uncertainty are represented by the terms σ_N^2, $\sigma_{\rm Mass}^2$, $\sigma_{\mu-z}^2$, $\sigma_{\rm lens}^2$, $\sigma_{\rm int}^2$, and $\sigma_{\rm Bias}^2$, respectively, in the equation

$$\sigma^2 = \sigma_N^2 + \sigma_{\rm Mass}^2 + \sigma_{\mu-z}^2 + \sigma_{\rm lens}^2 + \sigma_{\rm int}^2 + \sigma_{\rm Bias}^2 ,$$

The systematic matrix C_{sys} is a non-diagonal matrix that captures the correlation between different SNIa due to systematic effects. The details of how to construct this matrix can be found in Ref. [73].

4.2.2 Baryon acoustic oscillation

Baryon acoustic oscillations are recurring and periodic fluctuations in the density of visible baryonic matter. These oscillations are considered as "standard rulers" for the measurement of distances in cosmology. We employ data points from the following to constraint the cosmological parameters;

1. BOSS DR12 [74] at $z = 0.38, 0.51, 0.61$.
2. eBOSS DR14 (Lya) Combined [75, 76] at $z = 2.34$.
3. WiggleZ Dark Energy Survey [77] at $z = 0.44, 0.6$ and 0.73.

The Baryon Acoustic Oscillation (BAO) data provides valuable information about the angular diameter distance $d_{\rm A}(z)$ and the Hubble parameter $H(z)$. To obtain these values, we use the ratio d_z, which is defined as follows:

$$d_z \equiv \frac{r_{\rm s}\left(z_{\rm d}\right)}{D_V(z)}$$

where $D_V(z)$ represents the volume-averaged distance and is given by the expression:

$$D_V(z) = \left[(1+z)^2 d_{\rm A}^2(z)\frac{cz}{H(z)}\right]^{1/3}$$

The quantity $r_{\rm s}\left(z_{\rm d}\right)$ represents the comoving sound horizon at the drag epoch, and is defined as:

$$r_{\rm s}\left(z_{\rm d}\right) = \frac{1}{H_0}\int_{z_{\rm d}}^{\infty}\frac{c_{\rm s}(z)}{H(z)/H_0}\,{\rm d}z$$

Here, $c_{\rm s}(z)$ denotes the sound speed, and $z_{\rm d}$ is the redshift at the drag epoch and for the ΛCDM model, above equation can be approximated as [78, 79]:

$$r_{\rm s}\left(z_{\rm d}\right) \simeq \frac{44.5\log\left(\frac{9.83}{\Omega_{\rm m,0}h^2}\right)}{\sqrt{1+10\left(\Omega_{\rm b,0}h^2\right)^{3/4}}}{\rm Mpc}$$

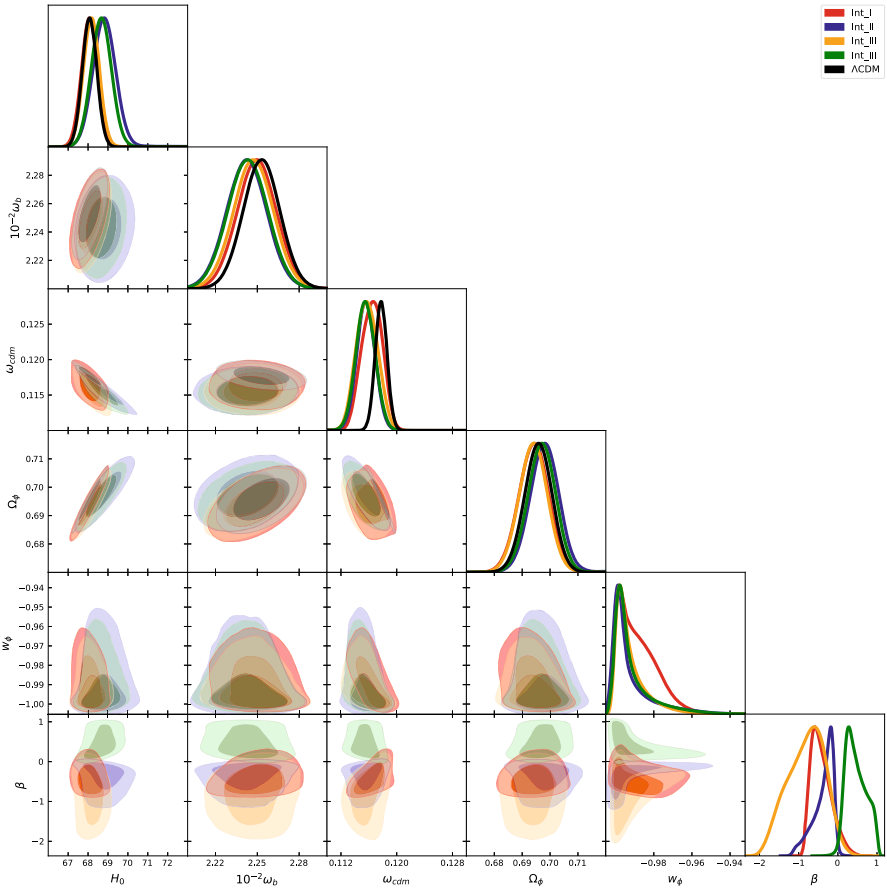

Fig. 3 A triangular plot shows the constraints on cosmological parameters for four different interactions, with the ΛCDM model's constraints shown in black for comparison

In the data sets, the value $\Omega_{b,0}h^2 = 0.0222$ from Planck18 [80] is considered unless otherwise specified.

4.2.3 Compressed planck likelihood

Because of the limitation on the computational resources, we have utilized the approach suggested by [81] in the compressed Planck likelihood to estimate the baryon physical density $\omega_b = \Omega_b h^2$ and the two shift parameters. For a more detailed explanation, please refer to Appendix A. The two shift parameters are given by:

$$\theta_* = r_s\left(z_{\rm dec}\right)/D_A\left(z_{\rm dec}\right), \quad \mathcal{R} = \sqrt{\Omega_M H_0^2}D_A\left(z_{\rm dec}\right),$$

Table 1 68%CL constraint on the cosmological parameters from the combining data sets of Pantheon supernova survey [73], Baryon Acoustic Oscillations from the BOSS DR12 survey [74], Lyman-alpha forest data from the eBOSS DR14 survey [76], and the WiggleZ galaxy survey [77], along with the compressed Planck likelihood

Parameter	Λ CDM	Int1	Int2	Int3	Int4
$10^{-2}\omega_b$	2.253 ± 0.014	2.250 ± 0.017	2.243 ± 0.015	2.248 ± 0.017	2.243 ± 0.015
ω_{cdm}	0.11775 ± 0.00094	$0.1164^{+0.0016}_{-0.0014}$	$0.1154^{+0.0014}_{-0.0011}$	0.1157 ± 0.0018	0.1155 ± 0.0015
β	–	$-0.42^{+0.15}_{-0.32}$	$-0.37^{+0.30}_{-0.11}$	$-0.81^{+0.55}_{-0.41}$	$0.46^{+0.18}_{-0.33}$
Ω_ϕ	0.6958 ± 0.0053	$0.6946^{+0.0048}_{-0.0055}$	$0.6986^{+0.0045}_{-0.0055}$	$0.6943^{+0.0045}_{-0.0052}$	0.6971 ± 0.0055
Ω_m	0.3041 ± 0.0053	$0.3009^{+0.0059}_{-0.0053}$	$0.2917^{+0.0080}_{-0.0063}$	$0.2985^{+0.0063}_{-0.0057}$	0.2939 ± 0.0077
H_0	68.08 ± 0.41	$68.10^{+0.35}_{-0.41}$	$68.92^{+0.43}_{-0.65}$	$68.20^{+0.35}_{-0.42}$	68.68 ± 0.59
$w\phi$	-1	$-0.9884^{+0.0052}_{-0.012}$	$-0.99204^{+0.00038}_{-0.0086}$	$-0.9922^{+0.0015}_{-0.0082}$	$-0.99146^{+0.00066}_{-0.0089}$
$\lvert\ln B_{I\Lambda}\rvert$	–	1.6	2.7	2.4	2.7

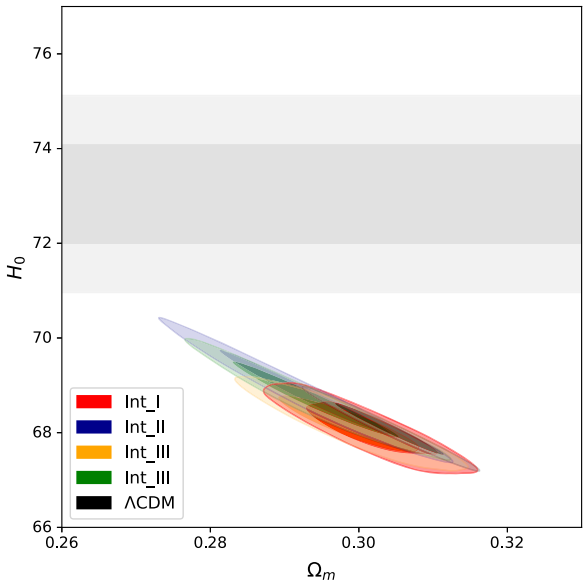

Fig. 4 A posterior plot of H_0 versus Ω_m demonstrates how the interacting models perform in resolving the Hubble tension. The horizontal gray band shows the constraint on the H_0 from SH0ES measurement [14]

Here, z_{dec} represents the redshift at decoupling, and D_A denotes the comoving angular diameter distance. We also confirmed that the compressed likelihood produces the standard Planck constraints for a flat ΛCDM model, as stated in [81].

4.3 Observational constraints

We assumed flat priors for both the cosmological ($100\ \omega_b$: $[1.9, 2.5]$, ω_{cdm} : $[0.095, 0.145]$) and model parameter ($\beta : [-1, 1]$). The α parameters which are related to the parametrization of the potential were assigned a prior of $[-2, 2]$. Based on [82], we set the sound horizon angular scale θ_s to the Planck CMB value of 1.04110 [80] and derive the current value of the Hubble parameter H_0. Fixing θ_s does not significantly affect the results since it is determined by the acoustic peak angular scales and is mostly independent of the CMB era physics.

The constrain at the 68%CL on the cosmological parameters together with the corresponding mean value are given in the Table.1 for the combined data sets of SN-Ia Pantheon compilation [73], BAO [74–77], with the compressed Planck likelihood [81]. In fig. 3 we have shown the 2D and 1D triangular plots of the cosmological parameters H_0, $100w_b$, w_{cdm}, Ω_ϕ, w_ϕ, β. A comparison with the ΛCDM model has been shown by plotting it in black. For all the interacting models $100w_b$, w_{cdm} are lower than the ΛCDM model.

In Fig. 4, we present a contour plot depicting the posterior distributions of the Hubble parameter H_0 and the matter density parameter Ω_m for all four interacting models together with the Λ CDM (in black) for comparison. The horizontal gray regions represent 1σ and 2σ constraint on the H_0 obtained from the SH0ES collaboration [14]. Notably, there is some increment in the current value of the Hubble parameter

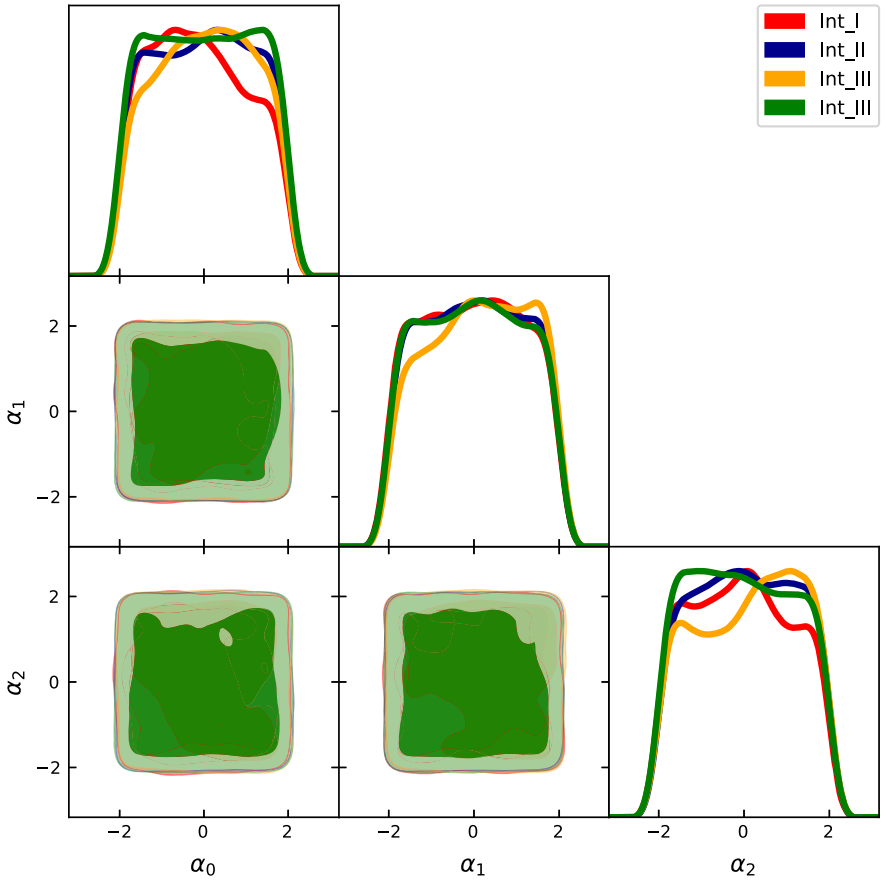

Fig. 5 A triangular posterior plot of the α parameters, with a prior range of $[-2, 2]$ for each parameter. One can notice there is no constraint on the α parameters

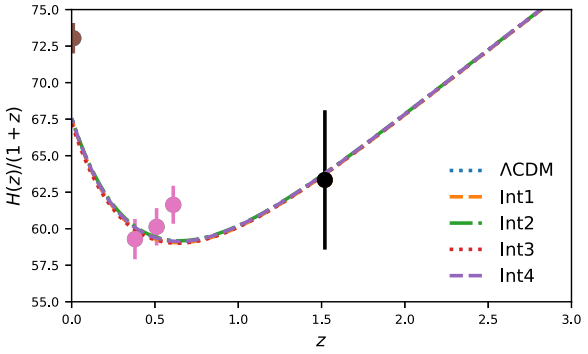

Fig. 6 A plot of $H(z)/(1+z)$ for the interacting models, using the same α parameter values as in Fig. 1, is presented along with observations from the Sh0ES survey [84] and Baryon Acoustic Oscillation (BAO) surveys [75, 85–87] for comparison

for all four models. To quantify the status of the tension in H_0 for these models, we utilize the estimator proposed in [83], which is given by

$$T_{H0} = \frac{\mid H_0 - H_0^{R18} \mid}{\sqrt{\sigma_{H0}^2 + \sigma_{\rm loc}^2}}, \tag{17}$$

where T_{H0} represents the tension, H_0 is the mean of the posterior $p(H_0)$, σ_{H0}^2 is the variance of the posterior $p(H_0)$, and $\sigma_{\rm loc}^2$ represents the uncertainty arising from local measurements. For interaction I, $T_{H0} \simeq 3.83\sigma$, for interaction II, $T_{H0} \simeq 3.51\sigma$, for interaction III, $T_{H0} \simeq 4.3\sigma$ and interaction IV $T_{H0} \simeq 3.64\sigma$. From the result of this estimator the performance of interaction II is better in terms of solving the Hubble tension.

Also, note from Table.1 that the value of the coupling parameter β is negative for interactions I to III, and positive for interaction IV. This is because interaction IV is linearly dependent on w_ϕ, and since w_ϕ is presently negative to counterbalance it, β is positive. However, from the signature of the coupling parameter β alone, one cannot conclude about the signature of the interaction term Q at present. To determine the signature of Q, one also needs to check the signature of $\dot{\phi}$. From Eq. (4a), we can write $\dot{\phi} = \frac{1}{\kappa}\sqrt{6}H\Omega_\phi^{1/2}\sin(\frac{1}{2}\cos^{-1}(-w_\phi))$, since $w_\phi = -\cos\theta$. It can be easily checked that for all the interacting models, $\dot{\phi} > 0$ once we consider the corresponding mean value of w_ϕ from Table 1, and hence $Q < 0$. This indicates a transfer of energy from dark energy to dark matter at present, which is opposite to the expectation for an accelerating universe.

Figure 5 shows the posteriors for the α parameters, and it can be observed that the α parameters remain unconstrained for all the interacting models, which is consistent with previous findings [62, 70].

In Fig. 6, we have plotted the expansion rate of the universe $H(z)/(1+z)$ as a function of z. For comparison, we have also shown observational data from Sh0ES [84] and BAO observations [75, 85–87]. From this plot, it can be seen that these interacting models can replicate the Λ CDM model well.

4.4 Comparison with ΛCDM

To be certain about the performance of the interacting models we compared the interacting models to the ΛCDM model using the Bayes factor, which was calculated as $\ln B_{I\Lambda} = \ln \mathcal{Z}I - \ln \mathcal{Z}\Lambda$, where $\mathcal{Z}$ represents the Bayesian evidence and the suffixes I and Λ represent the interacting models and ΛCDM models, respectively. To determine the preference for one model over another, we used Jeffrey's scale. A negative preference was assigned if $|\ln B_{I\Lambda}| < 1$, while positive, moderate, and strong preferences were assigned if $|\ln B_{I\Lambda}| > 1$, $|\ln B_{I\Lambda}| > 2.5$, and $|\ln B_{I\Lambda}| > 5.0$, respectively [88]. **Computation of the Bayesian Evidence for a model with high dimension parameter space is challenging as it involves integral over the whole parameter space. In this work, we have used the publicly available code** MCEVIDENCE [89] **to directly calculate the Bayes factor from the MCMC chains generated by** MON-

TEPYTHON **with the assumption that points in the chain are independent and using kth nearest-neighbour distance together with Mahalanobis distance metric. There are several other methods of model selection in cosmology. For a detailed discussion on this topic please see** [90], **where a comparative study of different selection methods has been presented.** Our analysis shows positive evidence for all of the interacting models over ΛCDM (see Table.1). According to Jeffrey's scale, Int1 and Int3 show positive evidence, whereas Int2 and Int4 show moderate evidence over the ΛCDM model.

5 Conclusions

In this study, we have explored the possibility of the interacting quintessence dark energy models as the alternative to the ΛCDM model. The choice of the type of interaction is phenomenological and also mathematically motivated to close the autonomous system. A general parametrization of the quintessence potential has been considered to study a large class of the potential in a single setup.

The Einstein field equations were reformulated into autonomous equations, and the models were implemented in the Boltzmann code CLASS and evaluated against recent cosmological observations. The state-of-the-art cosmological data sets are used to constrain the cosmological parameters of these models. Our finding suggests that even if there is a shift in the best-fit value of the H_0 towards the higher value but these models are far from solving the Hubble tension.

The cosmological evolution of the interacting models can well replicate the ΛCDM model at the background level but to be certain the results were compared using Bayesian model selection based on the Bayes factor and Jeffreys scale, providing insight into the relative strengths and weaknesses of these models. The study found that the interacting models are more favored by observations compared to ΛCDM. Out of the four interactions considered here, two show positive evidence, and the other two show moderate evidence over ΛCDM. We must mention here that current work is limited to the background level, in principle one should consider the evolution of the linear perturbations for a better understanding of these models which will be presented elsewhere in the future.

Acknowledgements The author acknowledges the use of the Chalawan High Performance Computing cluster, operated and maintained by the National Astronomical Research Institute of Thailand (NARIT).

Declarations

Funding The research is supported by Mahidol University, Thailand through the research project MU-MRC-MGR 04/2565.

Conflict of interest The authors have no relevant financial or non-financial interests to disclose.

References

1. Riess, A.G., et al.: Observational evidence from supernovae for an accelerating universe and a cosmological constant. Astron. J. **116**, 1009–1038 (1998)
2. Perlmutter, S., et al.: Measurements of Ω and Λ from 42 high redshift supernovae. Astrophys. J. **517**, 565–586 (1999)
3. Meszaros, A.: On the reality of the accelerating universe. Astrophys. J. **580**, 12–15 (2002)
4. Arnaud, M., et al.: Planck intermediate results. XXXI. Microwave survey of Galactic supernova remnants. Astron. Astrophys. **586**, A134 (2016)
5. Ahn, C.P., Alexandroff, R., Prieto, C.A., Anderson, S.F., Anderton, T., Andrews, B.H., Aubourg, É., Bailey, S., Balbinot, E., Barnes, R., et al.: The ninth data release of the sloan digital sky survey: first spectroscopic data from the sdss-iii baryon oscillation spectroscopic survey. Astrophys. J. Suppl. Ser. **203**(2), 21 (2012)
6. Padmanabhan, T.: Dark energy: mystery of the millennium. In AIP Conference Proceedings, volume 861, pages 179–196. American Institute of Physics, (2006)
7. Aghanim, N., et al.: Planck 2018 results. VI. Cosmological parameters. Astron. Astrophys. **641**, A6 (2020). [Erratum: Astron.Astrophys. 652, C4 (2021)]
8. Alam, S., Ata, M., Bailey, S., Beutler, F., Bizyaev, D., Blazek, J.A., Bolton, A.S., Brownstein, J.R., Burden, A., Chuang, C.-H., et al.: The clustering of galaxies in the completed sdss-iii baryon oscillation spectroscopic survey: cosmological analysis of the dr12 galaxy sample. Mon. Not. R. Astron. Soc. **470**(3), 2617–2652 (2017)
9. Beutler, F., Blake, C., Colless, M., Jones, D.H.: Lister staveley-smith, lachlan campbell, quentin parker, will saunders, and fred watson. The 6df galaxy survey: baryon acoustic oscillations and the local hubble constant. Mon. Not. Roy. Astron. Soci. **416**(4), 3017–3032 (2011)
10. Alam, S., Aubert, M., Avila, S., Balland, C., Bautista, J.E., Bershady, M.A., Bizyaev, D., Blanton, M.R., Bolton, A.S., Bovy, J., et al.: Completed sdss-iv extended baryon oscillation spectroscopic survey: cosmological implications from two decades of spectroscopic surveys at the apache point observatory. Phys. Rev. D, 103(8) (2021)
11. Abbott, T.M.C., et al.: Dark energy survey year 1 results: cosmological constraints from galaxy clustering and weak lensing. Phys. Rev. D **98**(4), 043526 (2018)
12. Macaulay, E., et al.: First cosmological results using type Ia supernovae from the dark energy survey: measurement of the hubble constant. Mon. Not. Roy. Astron. Soc. **486**(2), 2184–2196 (2019)
13. Krause, E., et al.: Dark energy survey year 1 results: multi-probe methodology and simulated likelihood analyses 6 (2017)
14. Riess, A.G., Casertano, S., Yuan, W., Macri, L.M., Scolnic, D.: Large magellanic cloud cepheid standards provide a 1% foundation for the determination of the hubble constant and stronger evidence for physics beyond λcdm. Astrophys. J. **876**(1), 85 (2019)
15. Wong, K.C., et al.: H0LiCOW—XIII. A 2.4 percent measurement of H0 from lensed quasars: 5.3 σ tension between early- and late-Universe probes. Mon. Not. Roy. Astron. Soc. **498**(1), 1420–1439 (2020)
16. Riess, A.G., Breuval, L., Yuan, W., Casertano, S., Macri, L.M., Bowers, J.B., Scolnic, D., Cantat-Gaudin, T., Anderson, R.I., Reyes, M.C.: Cluster cepheids with high precision gaia parallaxes, low zero-point uncertainties, and hubble space telescope photometry. Astrophys. J. **938**(1), 36 (2022)
17. Amendola, L., Tsujikawa, S.: Dark Energy: Theory and Observations. Cambridge University Press, Cambridge (2010)
18. Bamba, K., Capozziello, S., Nojiri, S., Odintsov, S.D.: Dark energy cosmology: the equivalent description via different theoretical models and cosmography tests. Astrophys. Space Sci. **342**, 155–228 (2012)
19. Copeland, E.J., Sami, M., Tsujikawa, S.: Dynamics of dark energy. Int. J. Mod. Phys. D **15**(11), 1753–1935 (2006)
20. Peebles, P.J.E., Ratra, B.: Quintessence: a review. Rev. Mod. Phys. **75**(2), 559–606 (2003)
21. Armendariz-Picon, C., Mukhanov, V., Steinhardt, P.J.: k-Essence as a model for dark energy. Phys. Rev. Lett. **85**(15), 4438–4441 (2001)
22. Roy, N., Goswami, S., Das, S.: Quintessence or phantom: study of scalar field dark energy models through a general parametrization of the hubble parameter. Phys. Dark Univ. **36**, 101037 (2022)
23. Banerjee, A., Cai, H., Heisenberg, L.: Hubble sinks in the low-redshift swampland. Phys. Rev. D **103**(8), L081305 (2021)

24. Lee, B.-H., Lee, W., Colgáin, E., Sheikh-Jabbari, M.M., Thakur, S.: Is local H $_0$ at odds with dark energy EFT? JCAP **04**(04), 004 (2022)
25. Krishnan, C., Colgáin, E.Ó., Sheikh-Jabbari, M.M., Yang, T.: Running Hubble tension and a H0 diagnostic. Phys. Rev. D **103**(10), 103509 (2021)
26. Roy, N., Banerjee, N.: Tracking quintessence: a dynamical systems study. Gen. Relativ. Gravit **46**, 1651 (2014)
27. Roy, N., Bhadra, N.: Dynamical systems analysis of phantom dark energy models. JCAP **1806**, 002 (2018)
28. Cedeño, F.X.L., Roy, N., Ureña-López, L.A.: Tracker phantom field and a cosmological constant: dynamics of a composite dark energy model (2021)
29. Karwal, T., Kamionkowski, M.: Dark energy at early times, the Hubble parameter, and the string axiverse. Phys. Rev. D **94**(10), 103523 (2016)
30. Peracaula, J.S., Gomez-Valent, A., Perez, J.D.C., Moreno-Pulido, C.: Running vacuum in the universe: phenomenological status in light of the latest observations, and its impact on the σ_8 and H_0 Tensions. Universe **9**(6), 262 (2023)
31. Rezaei, M., Sola Peracaula, J.: Running vacuum versus holographic dark energy: a cosmographic comparison. Eur. Phys. J. C **82**(8), 765 (2022)
32. Rezaei, M., Malekjani, M., Sola, J.: Can dark energy be expressed as a power series of the Hubble parameter? Phys. Rev. D **100**(2), 023539 (2019)
33. Rezaei, M., Peracaula, J.S., Malekjani, M.: Cosmographic approach to Running Vacuum dark energy models: new constraints using BAOs and Hubble diagrams at higher redshifts. Mon. Not. Roy. Astron. Soc. **509**(2), 2593–2608 (2021)
34. Valentino, E.D., Mukherjee, A., Sen, A.A.: Dark Energy with Phantom Crossing and the H_0 tension (2020)
35. Cai, R.-G., Wang, A.: Cosmology with interaction between phantom dark energy and dark matter and the coincidence problem. JCAP **03**, 002 (2005)
36. Mangano, G., Miele, G., Pettorino, V.: Coupled quintessence and the coincidence problem. Mod. Phys. Lett. A **18**(12), 831–842 (2003)
37. Sadjadi, H.M., Alimohammadi, M.: Cosmological coincidence problem in interactive dark energy models. Phys. Rev. D **74**, 103007 (2006)
38. Wang, B., Abdalla, E., Atrio-Barandela, F., Pavon, D.: Dark matter and dark energy interactions: theoretical challenges, cosmological implications and observational signatures. Rep. Prog. Phys. **79**(9), 096901 (2016)
39. Jesus, J.F., Escobal, A.A., Benndorf, D., Pereira, S.H.: Can dark matter–dark energy interaction alleviate the cosmic coincidence problem? Eur. Phys. J. C **82**(3), 273 (2022)
40. Salvatelli, V., Marchini, A., Pogosian, L., Vittorio, N., Wu, Y.-C., Zavala, J.: Indications of a late-time interaction in the dark sector. Phys. Rev. Lett. **113**(18), 181301 (2014)
41. Costa, A., Ferreira, P.G.: Hubble tension and interacting dark energy. J. Cosmol. Astropart. Phys. **2017**(12), 013 (2017)
42. Di Valentino, E., Melchiorri, A., Silk, J.: Cosmological constraints from the combination of latest data sets: the role of dark energy interactions. Eur. Phys. J. C **79**(2), 139 (2019)
43. Kumar, S., Kumar, S., Liao, K., Wang, Y.: Interacting dark energy models with a logarithmic interaction term and their implications on the hubble tension. Astrophys. Space Sci. **365**(6), 207 (2020)
44. Di Valentino, E., Melchiorri, A., Mena, O., Vagnozzi, S.: Interacting dark energy in the early 2020s: a promising solution to the H_0 and cosmic shear tensions. Phys. Dark Univ. **30**, 100666 (2020)
45. Di Valentino, E., Melchiorri, A., Mena, O., Vagnozzi, S.: Nonminimal dark sector physics and cosmological tensions. Phys. Rev. D **101**(6), 063502 (2020)
46. Yang, W., Pan, S., Di Valentino, E., Nunes, R.C., Vagnozzi, S., Mota, D.F.: Tale of stable interacting dark energy, observational signatures, and the H_0 tension. JCAP **1809**, 019 (2018)
47. Wang, D.: The multi-feature universe: Large parameter space cosmology and the swampland. Phys. Dark Univ. **28**, 100545 (2020)
48. Amendola, L.: Coupled quintessence. Phys. Rev. D **62**(4), 043511 (2000)
49. Farrar, G.R., Peebles, P.J.E.: Interacting dark matter and dark energy. Astrophys. J. **604**(1), 1 (2004)
50. Tamanini, N.: Phenomenological models of dark energy interacting with dark matter. Phys. Rev. D **92**(4), 043524 (2015)
51. Chimento, L.P.: Linear and nonlinear interactions in the dark sector. Phys. Rev. D **81**(4), 043525 (2010)

52. Pan, S., Bhattacharya, S., Chakraborty, S.: An analytic model for interacting dark energy and its observational constraints. Mon. Not. R. Astron. Soc. **452**(3), 3038–3046 (2015)
53. Pettorino, V., Baccigalupi, C., Mangano, G.: Extended quintessence with an exponential coupling. J. Cosmol. Astropart. Phys. **2005**(01), 014 (2005)
54. Pettorino, V., Baccigalupi, C.: Coupled and extended quintessence: theoretical differences and structure formation. Phys. Rev. D **77**(10), 103003 (2008)
55. Khyllep, W., Dutta, J., Basilakos, S., Saridakis, E.N.: Background evolution and growth of structures in interacting dark energy scenarios through dynamical system analysis. Phys. Rev. D **105**(4), 043511 (2022)
56. Caldera-Cabral, G., Maartens, R., Urena-Lopez, L.A.: Dynamics of interacting dark energy. Phys. Rev. D **79**, 063518 (2009)
57. Amendola, L.: Coupled quintessence. Phys. Rev. D **62**, 043511 (2000)
58. Boehmer, C.G., Caldera-Cabral, G., Lazkoz, R., Maartens, R.: Dynamics of dark energy with a coupling to dark matter. Phys. Rev. D **78**, 023505 (2008)
59. Zonunmawia, H., Khyllep, W., Roy, N., Dutta, J., Tamanini, N.: Extended phase space analysis of interacting dark energy models in loop quantum cosmology. Phys. Rev. D **96**(8), 083527 (2017)
60. Hussain, S., Chakraborty, S., Roy, N., Bhattacharya, K.: Dynamical systems analysis of tachyon-dark-energy models from a new perspective. Phys. Rev. D **107**(6), 063515 (2023)
61. Bahamonde, S., Böhmer, C.G., Carloni, S., Copeland, E.J., Fang, W., Tamanini, N.: Dynamical systems applied to cosmology: dark energy and modified gravity. Phys. Rep. **775–777**, 1–122 (2018)
62. Roy, N., Gonzalez-Morales, A.X., Urena-Lopez, L.A.: New general parametrization of quintessence fields and its observational constraints. Phys. Rev. D **98**(6), 063530 (2018)
63. Ureña-López, L.A., Gonzalez-Morales, A.X.: Towards accurate cosmological predictions for rapidly oscillating scalar fields as dark matter. JCAP **1607**(07), 048 (2016)
64. Ureña-López, L.A., Roy, N.: Generalized tracker quintessence models for dark energy. Phys. Rev. D **102**(6) (2020)
65. Wetterich, C.: The Cosmon model for an asymptotically vanishing time dependent cosmological 'constant'. Astron. Astrophys. **301**, 321–328 (1995)
66. Kumar, S., Nunes, R.C., Yadav, S.K.: Dark sector interaction: a remedy of the tensions between CMB and LSS data. Eur. Phys. J. C **79**(7), 576 (2019)
67. Lesgourgues, J.: The Cosmic Linear Anisotropy Solving System (CLASS) III: Comparision with CAMB for LambdaCDM (2011)
68. Blas, D., Lesgourgues, J., Tram, T.: The cosmic linear anisotropy solving system (CLASS) II: approximation schemes. JCAP **1107**, 034 (2011)
69. Lesgourgues, J., Tram, T.: The cosmic linear anisotropy solving system (CLASS) IV: efficient implementation of non-cold relics. JCAP **1109**, 032 (2011)
70. Roy, N., Bamba, K.: Arbitrariness of potentials in interacting quintessence models. Phys. Rev. D **99**(12), 123520 (2019)
71. Brinckmann, T., Lesgourgues, J.: MontePython 3: boosted MCMC sampler and other features (2018)
72. Reiss, A.G., et al.: Supernova serach team. Astron. J. **116**, 1009 (1998)
73. Scolnic, D.M., et al.: The complete light-curve sample of spectroscopically confirmed SNe Ia from Pan-STARRS1 and cosmological constraints from the combined pantheon sample. Astrophys. J. **859**(2), 101 (2018)
74. Alam, S., Ata, M., Bailey, S., Beutler, F., Bizyaev, D., Blazek, J.A., Bolton, A.S., Brownstein, J.R., Burden, A., Chuang, C.-H., et al.: The clustering of galaxies in the completed sdss-iii baryon oscillation spectroscopic survey: cosmological analysis of the dr12 galaxy sample. Mon. Not. R. Astron. Soc. **470**(3), 2617–2652 (2017)
75. Agathe, V.d.S., et al.: Baryon acoustic oscillations at z = 2.34 from the correlations of Lyα absorption in eBOSS DR14. Astron. Astrophys. **629**, A85 (2019)
76. Cuceu, A., Farr, J., Lemos, P., Font-Ribera, A.: Baryon acoustic oscillations and the hubble constant: past, present and future. J. Cosmol. Astropart. Phys. **2019**(10), 044–044 (2019)
77. Kazin, E.A., Koda, J., Blake, C., Padmanabhan, N., Brough, S., Colless, M., Contreras, C., Couch, W., Croom, S., Croton, D.J., et al.: The wigglez dark energy survey: improved distance measurements to z = 1 with reconstruction of the baryonic acoustic feature. Mon. Not. R. Astron. Soc. **441**(4), 3524–3542 (2014)
78. Eisenstein, D.J., Wayne, H.: Baryonic features in the matter transfer function. Astrophys. J. **496**, 605 (1998)

79. Martinelli, M., et al.: Euclid: forecast constraints on the cosmic distance duality relation with complementary external probes. Astron. Astrophys. **644**, A80 (2020)
80. Aghanim, N., et al.: Planck 2018 results. VI, Cosmological parameters (2018)
81. Arendse, N., Wojtak, R.J., Agnello, A., Chen, Geoff C.-F., Fassnacht, C.D., Sluse, D., Hilbert, S.M., Martin, B., Vivien, W., Kenneth, C., et al.: Cosmic dissonance: are new physics or systematics behind a short sound horizon? Astron. Astrophys. **639**, A57 (2020)
82. Sabti, N., Muñoz, J.B., Blas, D.: Galaxy luminosity function pipeline for cosmology and astrophysics. Phys. Rev. D **105**(4), 043518 (2022)
83. Camarena, D., Marra, V.: Impact of the cosmic variance on H_0 on cosmological analyses. Phys. Rev. D **98**(2), 023537 (2018)
84. Riess, A.G., Casertano, S., Yuan, W., Macri, L.M., Scolnic, D.: Large Magellanic cloud cepheid standards provide a 1% foundation for the determination of the hubble constant and stronger evidence for physics beyond ΛCDM. Astrophys. J. **876**(1), 85 (2019)
85. Alam, S., et al.: The clustering of galaxies in the completed SDSS-III Baryon Oscillation Spectroscopic Survey: cosmological analysis of the DR12 galaxy sample. Mon. Not. Roy. Astron. Soc. **470**(3), 2617–2652 (2017)
86. Zarrouk, P., et al.: The clustering of the SDSS-IV extended baryon oscillation spectroscopic survey dr14 quasar sample: measurement of the growth rate of structure from the anisotropic correlation function between redshift 0.8 and 2.2. Mon. Not. Roy. Astron. Soc. **477**(2), 1639–1663 (2018)
87. Blomqvist, M., et al.: Baryon acoustic oscillations from the cross-correlation of Lyα absorption and quasars in eBOSS DR14. Astron. Astrophys. **629**, A86 (2019)
88. Trotta, R.: Applications of Bayesian model selection to cosmological parameters. Mon. Not. Roy. Astron. Soc. **378**, 72–82 (2007)
89. Heavens, A., Fantaye, Y., Mootoovaloo, A., Eggers, H., Hosenie, Z., Kroon, S., Sellentin, E.: Marginal Likelihoods from Monte Carlo Markov Chains **4** (2017)
90. Rezaei, M., Malekjani, M.: Comparison between different methods of model selection in cosmology. Eur. Phys. J. Plus **136**(2), 219 (2021)